Nanoscale

Accepted Manuscript

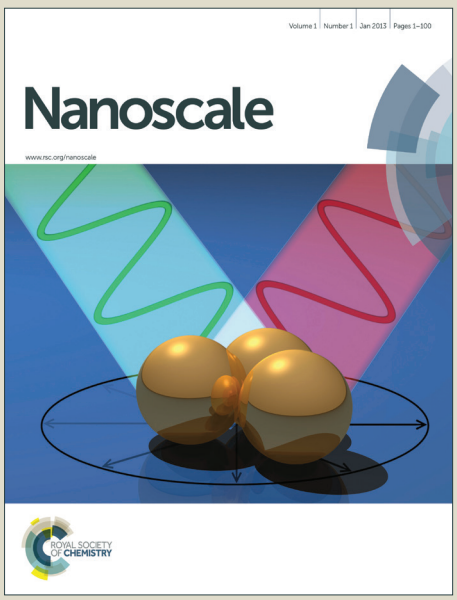

ROYAL SOCIETY OF CHEMISTRY

www.rsc.org/nanoscale

N-doped Graphitic Layers Encased Cobalt Nanoparticles as Efficient Oxygen Reduction Catalysts in Alkaline Media

Ce Han, Xiangjie Bo*, Yufan Zhang, Mian Li, Anaclet Nsabimana and Liping Guo*

Faculty of Chemistry, Northeast Normal University, Changchun, 130024, P. R. China

* Corresponding authors
Tel.: +86-0431-85099762.
Fax: +86-0431-85099762.
E-mail address: baoxj133@nenu.edu.cn (X. Bo), guolp078@nenu.edu.cn (L. Guo).

Nitrogen doped graphitic layers encased cobalt (N-C@Co) nanoparticles as novel non-precious-metal catalysts for the oxygen reduction reaction (ORR) were fabricated by a facile method using cyanamide and cobalt nitrate as precursors. The N-C@Co catalysts exhibited comparable catalytic performance, better stability and more excellent methanol tolerance towards ORR than those of commercial Pt/C catalyst.

Energy depletion problem is one of the major issues which hinder the development of human society. To solve this problem, fuel cells have received tremendous interests as a high-efficient and clean energy conversion device although their performance is still limited by the sluggish oxygen reduction reaction (ORR) at the cathode.[1] To date, platinum-based electrocatalysts have been considered as the most effective catalysts for the ORR, but they are still seriously restricted by the issues of high cost, insufficient durability, crossover effect, CO poisoning and limited natural storage.[2] Meanwhile, extensive research has been focused on reducing Pt consumption by developing Pt-based alloys;[3] however, the cost is still too high for commercialization. Therefore, the synthesis of durable and highly active non-precious catalysts becomes an imperative to realize the practical application of fuel cells.

During recent years, the research of alternative materials for Pt-based catalysts, such as non-precious-metal catalysts[4-7] and metal-free catalysts,[8-10] has attracted much attention. Transition-metal-based catalysts, such as iron (Fe), cobalt (Co), nickel (Ni), etc., are abundant in sources and have shown superior catalytic activity towards ORR.[11-13] In particular, the transitional metal oxides, carbides and nitrides have exhibited excellent high electrocatalytic performance towards ORR.[6, 12, 14-18] Recently, Xing *et al.* have synthesized hollow spheres of Fe_3C

nanoparticles encased in carbon as efficient oxygen reduction catalysts, further confirming that the transition-metal carbides can activate the carbon layer towards the ORR.[5] However, the zero valent metals in those materials have always been subjectively etched as the unstable constituent although they have shown impressive ORR activity. Thus, there is a great need to prevent the sustained dissolution and agglomeration of zero valent metals during the experiment. On the other hand, as metal-free catalysts, nitrogen-doped carbon materials have demonstrated surprisingly high electrocatalytic performance towards ORR.[8-10, 19, 20] It has been reported recently that the enhanced electrocatalytic activity could be attributed to the interaction between carbon atoms and neighboring N atoms which can create active sites for oxygen adsorption and reduction.[9, 21] However, the ORR activities of N-doped carbon materials are still less competitive compared to the Pt/C. Herein, we developed a facile method for the fabrication of N-doped carbon-shell coated Co (N-C@Co) nanoparticles and explored as non-precious-metal catalysts for the ORR. We expected that the N-doped carbon-shell should prevent the Co nanoparticles from the dissolution and agglomeration, meanwhile enhancing the electrocatalytic activity towards ORR. The synthesis of N-C@Co was accomplished by one-step pyrolysis using cyanamide and cobalt nitrate as precursors. As illustrated in Scheme 1, the fabrication process includes the mix of cyanamide and cobalt nitrate, polymerization of cyanamide under the relatively low temperature of the pyrolysis,[22] and carbonization of melamine encased Co nanoparticles under the high temperature of the pyrolysis. For comparison, three N-C@Co samples were obtained by keeping the mass of cobalt nitrate and adjusting the addition of cyanamide. Three N-C@Co samples with cyanamide addition of 2, 4 and 6 mL during the synthesis process were denoted as N-C@Co-1, N-C@Co-2 and N-C@Co-3, respectively. Cyanamide and cobalt nitrate were also respectively pyrolysed *via*

the same process. The detailed experimental process is shown in ESI.

The morphologies and microstructures of typical N-C@Co-2 and N-doped carbon (N-C, obtained by direct pyrolysis of cyanamide) were investigated by scanning electron microscopy (SEM) and transmission electron microscopy (TEM). As shown in Fig. 1a and c, the construct of N-C@Co-2 are nanoparticles with uniform size coated by the graphitic layers. This uniform dispersion of N-C@Co nanoparticles may be due to the carbon shell obtained by the carbonation of polymerized cyanamide (melamine). The formation of melamine avoids the agglomeration of Co nanoparticles and the emergence of oversized nanoparticles. However, the SEM and TEM images of N-C have not exhibited any specific morphology (Fig. 1b and d). Additionally, the graphitic structures of N-C@Co-2 and N-C further characterized from Raman spectroscopy are shown in Fig. S1. Compared with the N-C, the ratio of the D band (ca. 1380 cm^{-1}) to G band (ca. 1580 cm^{-1}) intensity (I_D/I_G) for N-C@Co-2 is much lower, reflecting a higher degree of graphitization. The presence of cobalt atom has been considered as the major factor in increase of graphitization degree.[4] The high-resolution TEM (HRTEM) images of N-C@Co-2 demonstrate that the Co nanoparticles are encased in six to twelve graphitic layers (Fig. 1e and Fig. S2).The graphitic shell has shown the lattice fringes with an interplanar spacing of 0.34 nm, corresponding to the (002) plane of graphite.[23] Meanwhile, in the core of nanoparticle, the well-defined crystalline lattice spacing of 0.21 nm can be clearly observed, consistent with the (111) plane of metallic cobalt.[24] This is in good agreement with the X-ray diffraction (XRD) analysis. Fig. 1f presents the XRD patterns of the N-C@Co-2 and the sample obtained by direct pyrolysis of cobalt nitrate. The diffraction peak at 26.6° corresponds to the (002) planes of graphite, while the peaks at 44.2° , 51.5° and 75.8° indicate the presence of metallic cobalt phase (JCPDS 15-0806).

Furthermore, as shown by cyan line in Fig. 1f, the XRD patterns are well accordant with diffraction peaks of cobalt oxide (CoO) species (JCPDS 65-2902). The metallic cobalt phase of the N-C@Co-2 should be derived from the reduction process of cobalt oxide phase by the graphite carbon phase at the high temperature of the pyrolysis. Therefore, the XRD results further confirm that the N-C@Co-2 is composed of the graphite carbon and metallic cobalt phases. In addition, considering the cyanamide applied as the carbon-nitrogen source, the absence of diffraction peaks for cobalt nitride in the XRD patterns demonstrates that the N atoms are solely doped into the graphite carbon shell rather than the cobalt core. Moreover, the sample obtained by direct pyrolysis of cobalt nitrate has been defined as CoO through the XRD analysis.

Through keeping the mass of cobalt nitrate and changing the addition of cyanamide, three N-C@Co samples were obtained and etched in 2 M HCl solution at 80 ºC for 12 hours to remove the incompletely encased cobalt nanoparticles. Here, N-C@Co-2 is taken as an example and the sample without acid etch is named as N-C@Co-2-ue. As shown in Fig. 2a, the XRD pattern of N-C@Co-2-ue exhibits unobvious difference compared to the N-C@Co-2. The result further demonstrates that the Co nanoparticles coated by carbon shell survive well after the etch procedure. The Brunauer–Emmett–Teller (BET) surface areas of the catalysts were measured, as shown in Fig. 2b and Fig S3. Results show that the N-C@Co-2 catalyst has a BET surface area of 261.0 m^2 g^{-1}, while the BET surface areas of N-C@Co-2-ue, N-C@Co-1 and N-C@Co-3 are 196.0, 68.1 and 145.4 m^2 g^{-1}, respectively. Compared with the N-C@Co-2-ue, the N-C@Co-2 has a higher BET surface area resulting from the loss of incompletely encased cobalt nanoparticles during the etch procedure.[25] Meanwhile, the relatively low BET surface areas of N-C@Co-1 and N-C@Co-3 are probably due to the overloading of Co atoms or the formation of overmuch

N-doped carbon resulting from the relatively surplus addition of cobalt nitrate or cyanamide. It seems clear that, the overloading of Co atoms leads to a decrease of porous carbon content, which further causing a drop in the BET surface area. On the other hand, the N-doped carbon obtained by direct pyrolysis of melamine with relatively low BET surface area has been reported by the published literature.[26] The pore-size distribution, calculated using the Barrett–Joyner–Halenda (BJH) method, shows little difference from all the N-C@Co catalysts (Fig S3b and the inset in Fig 2b), confirming that different ratios of cyanamide to cobalt nitrate have no effect on pore-size distribution.

X-ray photoelectron spectroscopy (XPS) was employed to reveal the element contents and the relative content of each component in the composite (Table S1). Based on the XPS data, three N-C@Co catalysts show similar mass ratios of carbon to nitrogen resulting from the cyanamide as sole carbon-nitrogen precursor. The XPS signals in the Co $2p_{3/2}$ region reveal the presence of Co (0) (Co1 at ~777.7 eV), cobalt oxide (Co2 at ~779.1 eV) and Co-C-N (Co3 at ~780.1 eV) (Fig. 2c and Fig S4).[4] According to the Table S1, the Co (0) content of three N-C@Co catalysts increases with the increasing addition of cyanamide, which is probably due to the reduction process of cobalt oxide by the graphite carbon. In addition, several published literatures have reported that the peak of Co-N is located around 781.6 ± 0.2 eV.[27, 28] Therefore, the XPS spectrum without Co-N peak further expounds the sole doping of N atoms into the carbon shell rather than the Co core. Moreover, the high-resolution N 1s scans can be fitted into four peaks at 398.1, 399.2, 400.7 and 404.6 eV, corresponding with the pyridinic-N (N1), pyrrolic-N (N2), graphitic-N (N3) and oxidized pyridinic-N (N4), respectively (Fig. 2d and Fig. S5).[29] As demonstrated in Table S1, the N-C@Co-2 has higher graphitic-N content than the N-C@Co-1 and N-C@Co-3. Among the four

components, graphitic-N specie has been considered more active towards ORR compared with the pyridinic-N, pyrrolic-N and oxidized pyridinic-N.[30]

To study the ORR electrocatalytic activities of samples, three-electrode cyclic voltammetry (CV) experiments in oxygen saturated 0.1 M KOH solutions were performed at a scan rate of 50 mV s^{-1}. As shown in Fig. S6, the N-C@Co-2 exhibits a distinct cathodic peak centered at 0.8V, which is more positive than that for other as-prepared catalysts except the commercial Johnson Matthey Pt/C catalyst (20 wt% Pt loading). The ORR electrocatalytic properties of these catalysts were further investigated by linear sweep voltammograms (LSV) using a rotating disk electrode (RDE) in O_2-saturated 0.1 M KOH electrolyte at a scanning rate of 5 mV s^{-1} and a rotation rate of 625 rpm (Fig. 3a and b). As shown in Fig. 3a, the N-C@Co-2 displays distinctly more positive onset potential (0.895 V) and higher current density than the N-C (0.815 V) and the CoO (0.645 V), further demonstrating the high ORR catalytic activity of N-C@Co-2 resulting from the particular N-doped carbon shell and cobalt nanoparticle core structure. Although the Co nanoparticle core is not in direct contact with the O_2-saturated solution, it still has a vital catalytic role for the ORR performance. As illustrated in Fig. 4, the coated metallic Co nanoparticles activate the N-doped graphitic shell, resulting in the more enhanced ORR performance of catalysts compared with that of sample without Co (N-C).[5] Moreover, the onset potential of Pt/C (0.905 V) is about 10 mV more positive than that of N-C@Co-2, indicating that N-C@Co-2 may have great potential to become an alternative material for Pt/C as noble-metal-free electrocatalyst for ORR. The sample without acid-etch (N-C@Co-2-ue) exhibits a more negative onset potential (0.855V) and lower current density than that of N-C@Co-2 (Fig. 3b). This result should be due to the higher BET surface area facilitating the exposure of active sites for catalysis. Meanwhile, Fig. 3b further

shows the impact of the cyanamide addition on the LSV responses for oxygen. It can be seen that the onset potential at N-C@Co-1 and N-C@Co-3 commences around 0.835 V and 0.855V, respectively. The improvement of the catalytic performance on the N-C@Co-2 electrode further confirms that the N-C@Co-2 has the best ORR activity owing to synergistic effect arising from the high surface area, active N specie, optimized N, Co content obtained by the adjustment of cyanamide addition.

To further confirm the active specie of Co core towards ORR, the XPS results of Co $2p_{3/2}$ analysis was taken together with the ORR catalytic activity of three N-C@Co catalysts. As demonstrated in Table S1, the N-C@Co-2 has a higher metallic Co content than the N-C@Co-1. Meanwhile, the N-C@Co-3 has a lower Co elementary content than the N-C@Co-2 although it has the highest metallic Co content. By taking these results into consideration, it may be readily deduced that the metallic Co specie is more active towards ORR compared with the CoO and Co-C-N.

To better understand the ORR electrochemical kinetics of N-C@Co-2, the RDE measurements at various rotating speeds were also performed to analyze the transferred electron number per O_2 molecule during reduction (n) (Fig. S7). A set of polarization curves for ORR on N-C@Co-2 catalyst recorded from 100 to 2025 rpm are displayed in Fig. S7a. These polarization curves show typical increasing current with higher rotating rates. The Koutecky-Levich (K-L) plots (Fig. S7b) are obtained from polarization curves at different potentials. Obviously, these plots are perfectly parallel and show good linearity over the entire potential range, which indicates that the electron transfer number for ORR is similar even at high potentials. The slopes of the K-L plots are used to calculate the electron transfer number during ORR on the basis of K-L equation

(details are shown in the ESI Equation 1 and 2). The electrochemical reduction of oxygen in alkaline solution proceeds through two main possible pathways, including the two-electron reduction pathway with HO_2^- as an intermediate product and the four-electron pathway to directly reduce to OH^-. The latter pathway is more efficient for energy conversion.[31] The *n* value calculated in the ORR for N-C@Co-2 was about 3.74-4.00 in the potential range from 0.715 to 0.265 V (Fig. S7c). Meanwhile, as a reference, the *n* value of Pt/C is similar to that of N-C@Co-2 and is shown in the same figure. To further confirm the ORR catalytic pathway, rotating ring disk electrode (RRDE) measurements were performed to investigate the HO_2^- yields and the *n* values during the ORR process at 900 rpm rotating speed (Fig. 3c). The equations used to analyze the RRDE data are shown in ESI Equation 3 and 4. The *n* value of N-C@Co-2 is stable at 3.8 to 3.9 over the potential range from 0.715 to 0.265 V, which is consistent with result obtained from the RDE experiments (Fig. 3d). Meanwhile, the HO_2^- yield of N-C@Co-2 was found to be less than 10 % at all potentials, indicating a four-electron pathway dominated ORR process by reducing oxygen directly to OH^- ions (Fig. 3e). The *n* value on N-C@Co-2 is close to 4, which further indicates that the N-C@Co-2 can efficiently reduce the oxygen molecule *via* a four-electron transfer pathway. In addition, as demonstrated by the RRDE experiments, the N-C@Co-2 exhibits excellent ORR performance comparable to that of Pt/C, confirming the great potential of this non-precious catalyst as a promising alternative to the Pt/C.

Given that catalyst durability is one of the major challenges for alkaline fuel cells, the durability of N-C@Co-2 and Pt/C catalyst for ORR was evaluated through chronoamperometric measurements at a constant voltage of 0.565 V *vs*. RHE for 30000 s of continuous operation in O_2-saturated 0.1 M KOH solution at a rotation speed of 900 rpm. As shown in Fig. S8a, the

current for ORR at the N-C@Co-2 electrode exhibits slow attenuation with a decay about 9.8 % of the initial current, while the Pt/C catalyst experiences about 34.2 % decrease in current density, revealing that the stability of N-C@Co-2 is superior to that of Pt/C in the alkaline medium. In addition to the durability, the possible crossover effect of the catalyst is another major concern to be emphasized for ORR. Thus, the electrocatalytic selectivity of N-C@Co-2 and Pt/C was measured in the presence of 3 M methanol by the CVs and the chronoamperometric responses at a potential of 0.565 V *vs*. RHE (Fig. S8b-d). The current-time curves in Fig. S8b illustrate that the oxygen reduction current for the Pt/C catalyst jump to positive values when methanol is introduced, whereas no noticeable response is observed in the ORR current at the N-C@Co-2 electrode under similar conditions. CV curves in Fig. S8c display a stable oxygen reduction current without the current towards methanol at the N-C@Co-2 electrode. While in contrast, a disappearance of the cathodic peak for ORR with the addition of methanol is observed at the Pt/C electrode, further confirming that Pt/C catalyst have a serious methanol crossover effect (Fig. S8d). On the basis of these studies, the N-C@Co-2 catalyst exhibits a remarkably better methanol tolerance and electrochemical stability than the Pt/C catalyst.

In summary, a novel ORR catalyst in form of Co nanoparticles encased by N-doped graphitic layers was successfully synthesized by a one-step pyrolysis process. Electrochemical experiments reveal that the ORR catalytic performance of as-prepared materials is improved by the synergistic effect arising from the adjustment of cyanamide addition and the particular N-doped carbon shell/ cobalt nanoparticle core structure. The N-doped graphitic shell stabilizes the Co nanoparticles avoiding the dissolution and agglomeration, meanwhile the Co nanoparticle core plays a positive role in activating the N-doped graphitic shell towards ORR. The N-C@Co-2 catalyst manifests

excellent ORR activity with highly positive onset potential in a four-electron transfer pathway approaching to that of Pt/C catalysts. Moreover, its enhanced stability and high electrocatalytic selectivity towards ORR make it promising as a low-cost and effective non-precious metal-based ORR catalyst. Our work paves a new way to design and synthetize alternative non-precious metal-based catalysts to the Pt-based catalysts towards ORR.

Acknowledgements

The authors gratefully acknowledge National Natural Science Foundation of China （21405011） and China Postdoctoral Science Foundation funded project（2014M550164）.

References

1. M. K. Debe, *Nature*, 2012, **486**, 43-51.
2. Z. Chen, D. Higgins, A. Yu, L. Zhang and J. Zhang, *Energy Environ. Sci.*, 2011, **4**, 3167-3192.
3. Y. Bing, H. Liu, L. Zhang, D. Ghosh and J. Zhang, *Chem. Soc. Rev.*, 2010, **39**, 2184-2202.
4. M. Li, X. Bo, Y. Zhang, C. Han, A. Nsabimana and L. Guo, *J. Mater. Chem. A*, 2014, **2**, 11672-11682.
5. Y. Hu, J. O. Jensen, W. Zhang, L. N. Cleemann, W. Xing, N. J. Bjerrum and Q. Li, *Angew. Chem. Int. Ed.*, 2014, **53**, 3675-3679.
6. Y. Liang, Y. Li, H. Wang, J. Zhou, J. Wang, T. Regier and H. Dai, *Nat Mater*, 2011, **10**, 780-786.
7. R. Liu, X. Yu, G. Zhang, S. Zhang, H. Cao, A. Dolbecq, P. Mialane, B. Keita and L. Zhi, *J. Mater. Chem. A*, 2013, **1**, 11961-11969.
8. X. Bo, C. Han, Y. Zhang and L. Guo, *ACS Appl. Mat. Interfaces*, 2014, **6**, 3023-3030.
9. K. Gong, F. Du, Z. Xia, M. Durstock and L. Dai, *Science*, 2009, **323**, 760-764.
10. D. Geng, Y. Chen, Y. Chen, Y. Li, R. Li, X. Sun, S. Ye and S. Knights, *Energy Environ. Sci.*, 2011, **4**, 760-764.
11. G. Zhang, B. Y. Xia, X. Wang and X. W. Lou, *Adv. Mater.*, 2014, **26**, 2408-2412.
12. H. Yin, C. Zhang, F. Liu and Y. Hou, *Adv. Funct. Mater.*, 2014, **24**, 2930-2937.
13. H. Zhu, S. Zhang, Y.-X. Huang, L. Wu and S. Sun, *Nano Lett.*, 2013, **13**, 2947-2951.
14. J.-S. Lee, G. S. Park, S. T. Kim, M. Liu and J. Cho, *Angew. Chem. Int. Ed.*, 2013, **52**, 1026-1030.
15. G. Wu, M. Nelson, S. Ma, H. Meng, G. Cui and P. K. Shen, *Carbon*, 2011, **49**, 3972-3982.
16. G. Wu, K. L. More, C. M. Johnston and P. Zelenay, *Science*, 2011, **332**, 443-447.
17. J. Wu, S. Dou, A. Shen, X. Wang, Z. Ma, C. Ouyang and S. Wang, *J. Mater. Chem. A*, 2014, **2**, 20990-20995.

18. Y. Yang, J. Liu, Y. Han, H. Huang, N. Liu, Y. Liu and Z. Kang, *PCCP*, 2014, **16**, 25350-25357.
19. R. Liu, H. Liu, Y. Li, Y. Yi, X. Shang, S. Zhang, X. Yu, S. Zhang, H. Cao and G. Zhang, *Nanoscale*, 2014, **6**, 11336-11343.
20. H. Wang, T. Maiyalagan and X. Wang, *ACS Catalysis*, 2012, **2**, 781-794.
21. L. Qu, Y. Liu, J.-B. Baek and L. Dai, *ACS Nano*, 2010, **4**, 1321-1326.
22. M. Groenewolt and M. Antonietti, *Adv. Mater.*, 2005, **17**, 1789-1792.
23. Z. Li, S. Ji, B. G. Pollet and P. K. Shen, *Chem. Commun.*, 2014, **50**, 566-568.
24. E. Higuchi, H. Otsuka, M. Chiku and H. Inoue, *J. Power Sources*, 2014, **248**, 762-768.
25. L. Zhang, H. B. Wu, B. Liu and X. W. Lou, *Energy Environ. Sci.*, 2014, **7**, 1013-1017.
26. H. Yan, Y. Chen and S. Xu, *Int. J. Hydrogen Energy*, 2012, **37**, 125-133.
27. B. Zheng, J. Wang, F.-B. Wang and X.-H. Xia, *J. Mater. Chem. A*, 2014, **2**, 9079-9084.
28. K. Niu, B. Yang, J. Cui, J. Jin, X. Fu, Q. Zhao and J. Zhang, *J. Power Sources*, 2013, **243**, 65-71.
29. J. Sanetuntikul, T. Hang and S. Shanmugam, *Chem. Commun.*, 2014, **50**, 9473-9476.
30. R. Liu, D. Wu, X. Feng and K. Müllen, *Angewandte Chemie*, 2010, **122**, 2619-2623.
31. S. Kattel, P. Atanassov and B. Kiefer, *PCCP*, 2013, **15**, 148-153.

Captions

Scheme 1 Schematic illustration of the fabrication procedure for N-doped graphitic layers encased cobalt nanoparticles (N-C@Co) catalysts

Fig.1 SEM images of N-C@Co-2 (a) and N-C (b). TEM images of N-C@Co-2 (c) and N-C (d). HRTEM image of an N-doped graphitic layers encased Co nanoparticle in N-C@Co-2 (e). The inset in (e) is the corresponding index crystal plane. XRD patterns of N-C@Co-2 and CoO (f).

Fig.2 XRD patterns of N-C@Co-2 and N-C@Co-2-ue (a). Nitrogen adsorption-desorption isotherms of N-C@Co-2 and N-C@Co-2-ue (b). Inset: Pore size distributions of N-C@Co-2 and N-C@Co-2-ue. High-resolution XPS Co $2p_{3/2}$ (c) and N 1s (d) spectra of N-C@Co-2.

Fig.3 RDE LSV curves of CoO, N-C, N-C@Co-2 and Pt/C at scan rate of 5 mV s^{-1} and a rotation speed of 625 rpm in O_2-saturated 0.1 M KOH (a). RDE LSV curves of

N-C@Co-2-ue, N-C@Co-1, N-C@Co-2 and N-C@Co-3 at scan rate of 5 mV s^{-1} and a rotation speed of 625 rpm in O_2-saturated 0.1 M KOH (b). The RRDE ring current and disk current of the N-C@Co-2 and Pt/C recorded in oxygen-saturated 0.1 M KOH at a scan rate of 5 mV s^{-1} and a rotation rate of 900 rpm (c). The ring potential of Pt ring is constant at 1.465 V *vs.*RHE. The electron transfer number (d) and the HO_2^- yield (e) of the N-C@Co-2 and Pt/C catalysts for the ORR in 0.1 M KOH.

Fig. 4 The ORR procedure on the N-C@Co-2 electrode.

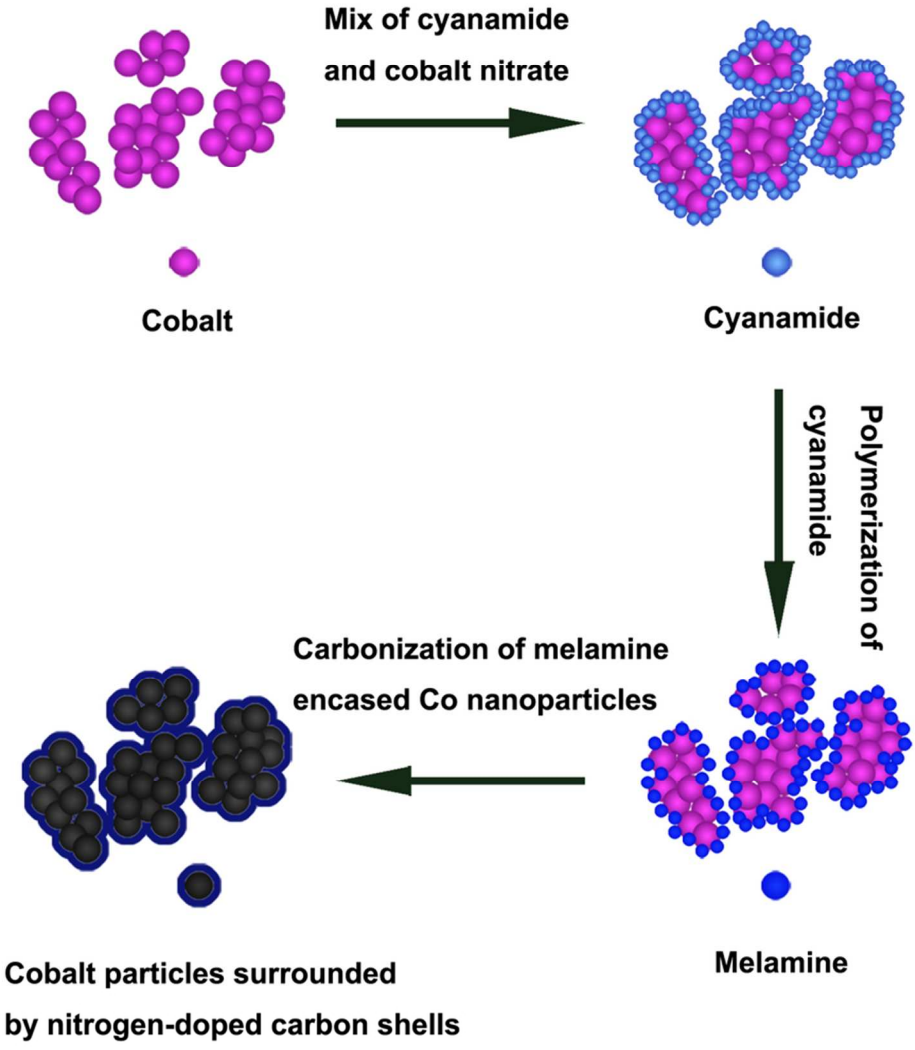

Schematic illustration of the fabrication procedure for N-doped graphitic layers encased cobalt nanoparticles (N-C@Co) catalysts.
80x89mm (300 x 300 DPI)

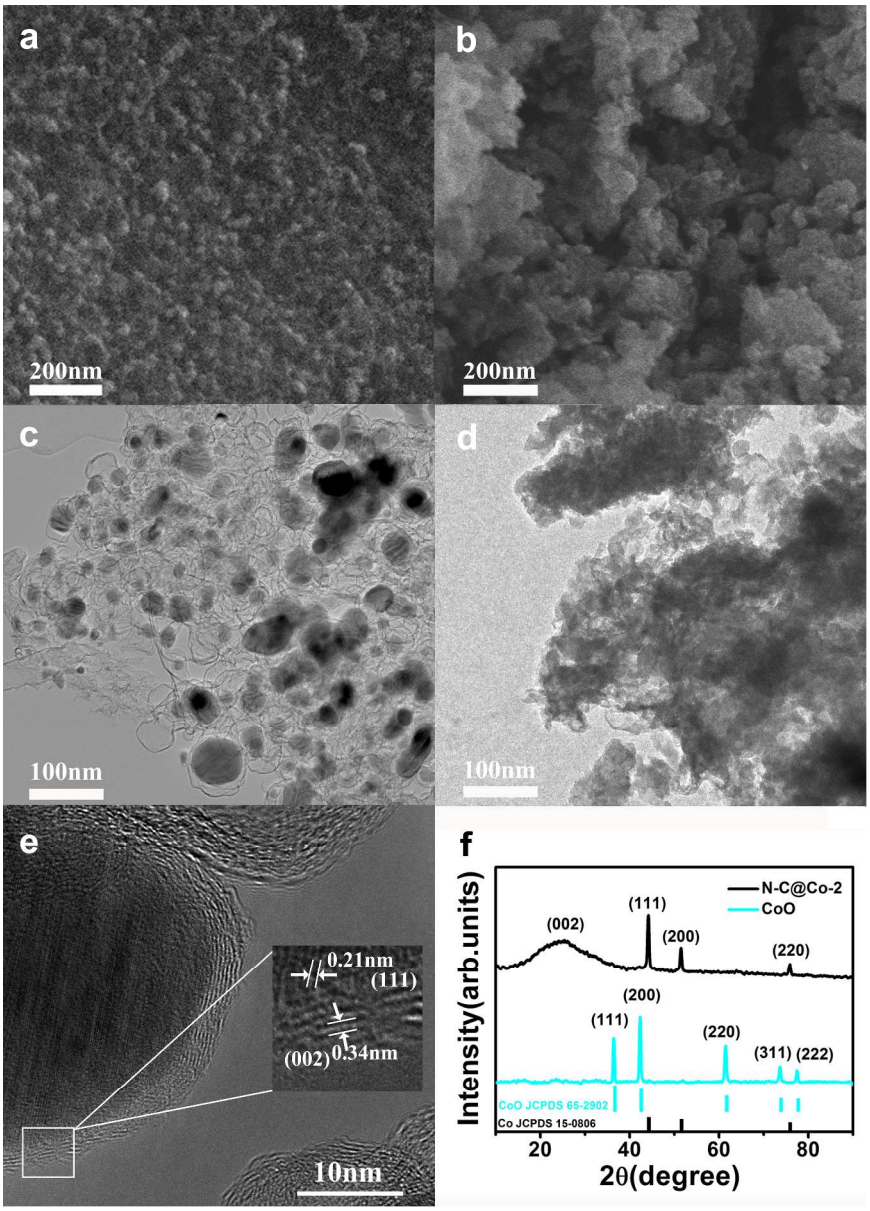

Fig.1 SEM images of N-C@Co-2 (a) and N-C (b). TEM images of N-C@Co-2 (c) and N-C (d). HRTEM image of an N-doped graphitic layers encased Co nanoparticle in N-C@Co-2 (e). The inset in (e) is the corresponding index crystal plane. XRD patterns of N-C@Co-2 and CoO (f).

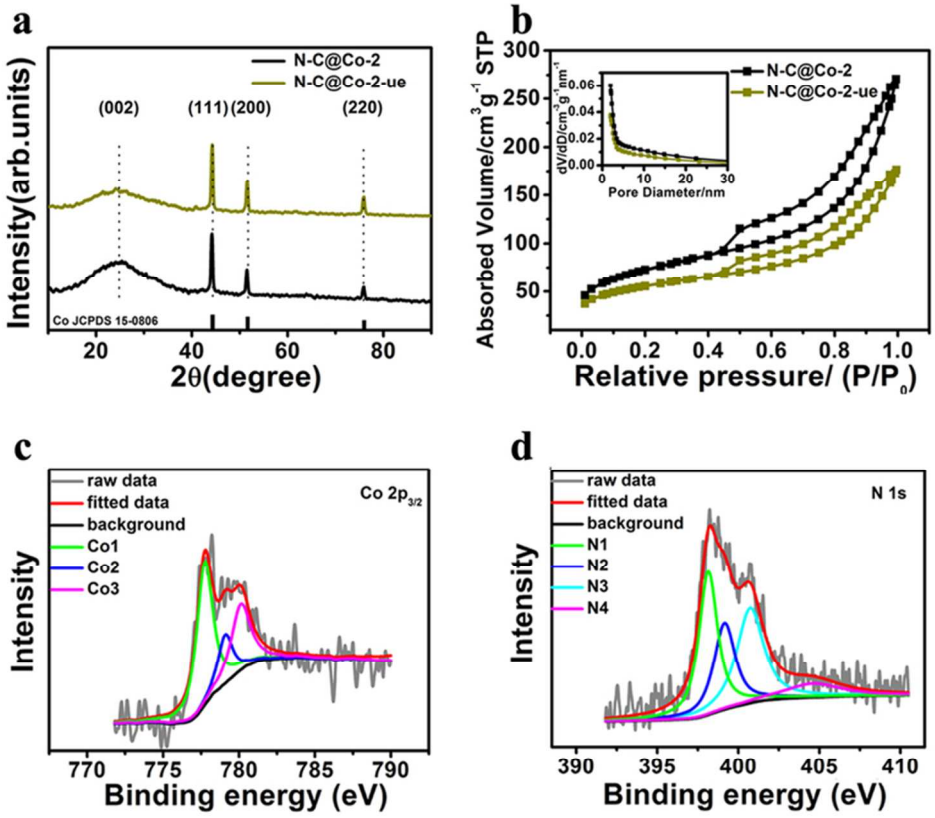

Fig.2 XRD patterns of N-C@Co-2 and N-C@Co-2-ue (a). Nitrogen adsorption-desorption isotherms of N-C@Co-2 and N-C@Co-2-ue (b). Inset: Pore size distributions of N-C@Co-2 and N-C@Co-2-ue. High-resolution XPS Co 2p3/2 (c) and N 1s (d) spectra of N-C@Co-2.
69x59mm (300 x 300 DPI)

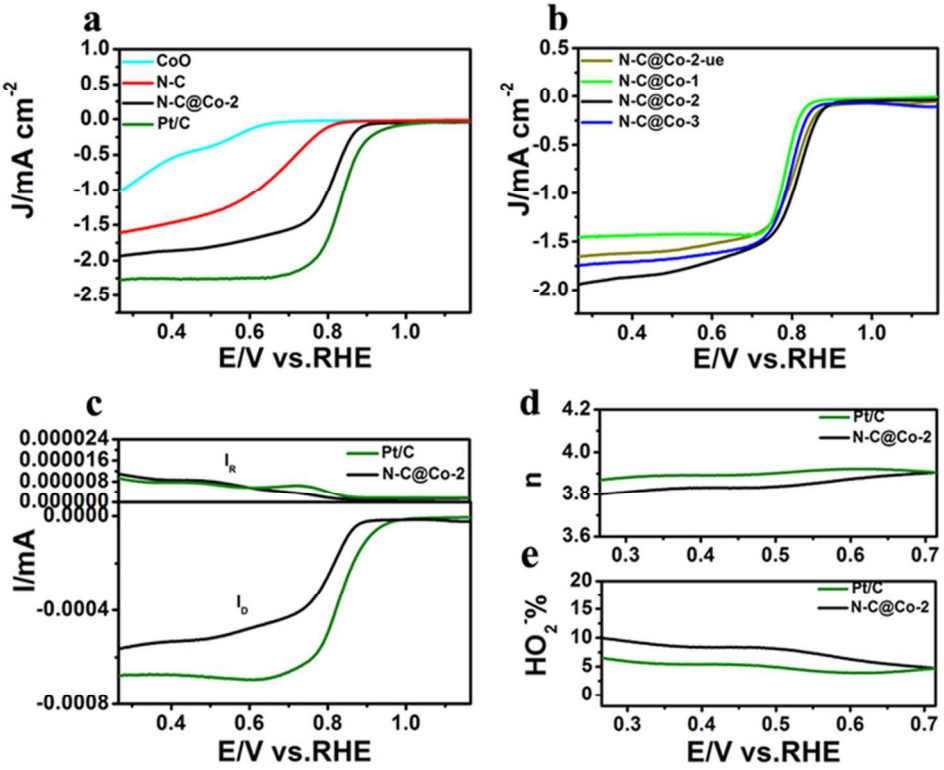

Fig.3 RDE LSV curves of CoO, N-C, N-C@Co-2 and Pt/C at scan rate of 5 mV s-1 and a rotation speed of 625 rpm in O2-saturated 0.1 M KOH (a). RDE LSV curves of N-C@Co-2-ue, N-C@Co-1, N-C@Co-2 and N-C@Co-3 at scan rate of 5 mV s-1 and a rotation speed of 625 rpm in O2-saturated 0.1 M KOH (b). The RRDE ring current and disk current of the N-C@Co-2 and Pt/C recorded in oxygen-saturated 0.1 M KOH at a scan rate of 5 mV s-1 and a rotation rate of 900 rpm (c). The ring potential of Pt ring is constant at 1.465 V vs.RHE. The electron transfer number (d) and the HO2- yield (e) of the N-C@Co-2 and Pt/C catalysts for the ORR in 0.1 M KOH.
64x51mm (300 x 300 DPI)

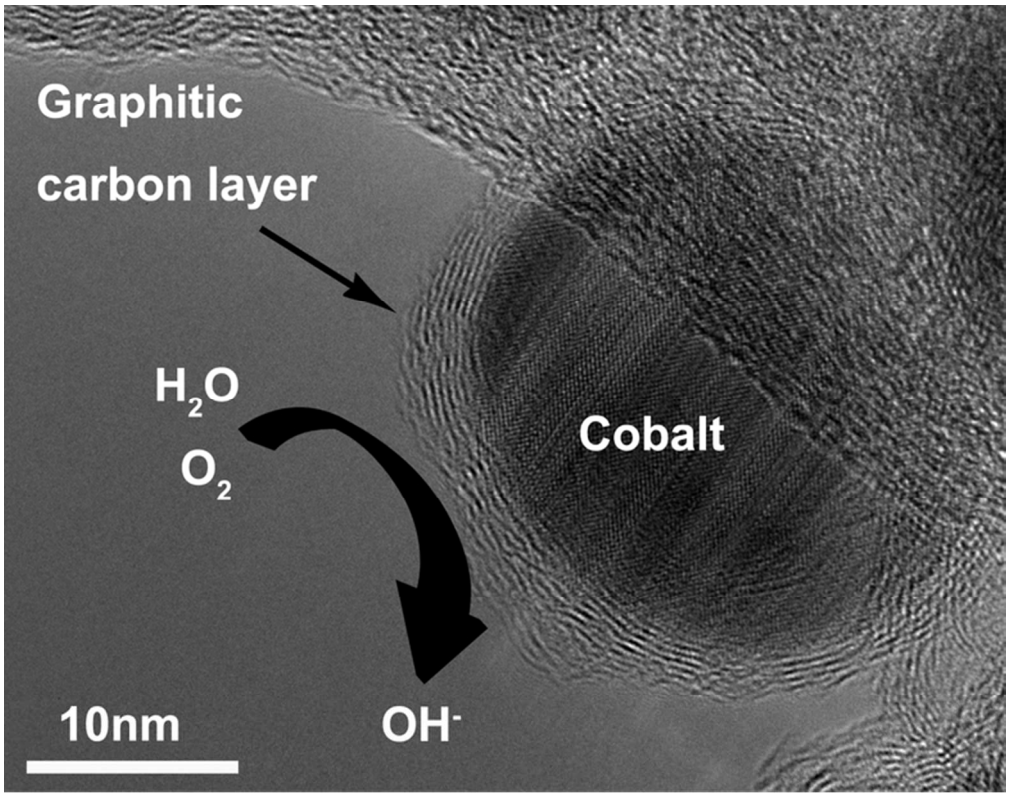

The ORR procedure on the N-C@Co-2 electrode.
66x51mm (300 x 300 DPI)